STUDY OF ELECTROMAGNETIC DECAYS AT CERN

D. Bollini, P. Dalpiaz, T. Massam, F. Navach,
F.L. Navarria, M.A. Schneegans and A. Zichichi

CERN, Geneva, Switzerland
Istituto di Fisica dell'Università, Bologna, Italy
Istituto Nazionale di Fisica Nucleare, Sezione di Bologna, Italy
Centre de Recherches Nucléaires, Strasbourg, France

Invited paper, presented by A. Zichichi

1. INTRODUCTION

The purpose of this paper is to give a review of the results obtained by the CERN-Bologna neutron missing-mass spectrometer, in the field of electromagnetic decays of mesons. In fact, the experimental set-up has great flexibility and can be used to investigate the reaction

$$\pi^- + p \rightarrow n + M^0 \qquad (1)$$

$M^0 \rightarrow$ anything
$M^0 \rightarrow$ neutrals only
$M^0 \rightarrow e^+e^-$
$M^0 \rightarrow \gamma\gamma$

where M^0 is any sort of neutral particle produced in $(\pi^- p)$ interactions. For completeness, the physics program we had in mind when the set-up was designed is listed below:

1. Study of the differential cross-section for meson production.
2. Decay branching ratios of the various M^0's.
3. Search for neutral resonances.
4. $\phi \rightarrow e^+e^-$ → ω-φ mixing angle
5. $\omega \rightarrow e^+e^-$ → ω-φ mixing angle
6. Search for γ decay modes of neutral resonances.

7. $\omega \to \pi^+\pi^-$.

8. $\phi \to \pi^+\pi^-$.

The results obtained during 4¾ weeks of CERN-PS running time are the following:

1. Production of η: $d\sigma/d\Omega$ at three angles, for $P_\pi = 0.81$ GeV/c.

2. Production of ω: $d\sigma/d\Omega$ at four angles, for $P_\pi = 2.12$ GeV/c.

3. Production of φ: $d\sigma/d\Omega$ integrated over $0.00 \leq \cos\theta^* \leq 0.95$, for $P_\pi = 2.13$ GeV/c.

4. Branching ratio: $\omega \to$ neutrals/$\omega \to$ total.

5. Branching ratio: $\eta \to$ neutrals/$\eta \to$ total.

6. Evidence against the existence of the S^0 meson.

7. (e^+e^-) decay of the φ mesons → (ω-φ) mixing angle

8. (e^+e^-) decay of the ω meson → (ω-φ) mixing angle

9. X^0 decay to γγ.

10. Search for $\omega \to \pi^+\pi^-$.

11. Search for $\phi \to \pi^+\pi^-$.

The present paper will discuss only points 7, 8, and 9.

2. THE EXPERIMENTAL SET-UP

A schematic diagram of the experimental set-up is shown in Fig. 1. It consists of the following:

i) A system of "beam-defining counters" $\check{C}U\bar{S}R$: $\check{C}$ is a gas Čerenkov counter to anticoincide the electrons present in the primary beam; U is an important plastic scintillator counter used in the timing of the neutron; S is a very thin (0.05 cm) plastic scintillation counter, used to reduce as much as possible the interactions outside the H_2 target; R is an anticoincidence counter to remove beam halo.

ii) A 40 cm long, 5 cm diameter H_2 target. A veto counter, not shown in this drawing, is placed behind the target in order to anticoincide non-interacting pions.

iii) Two electromagnetic shower detectors, called electron "top" and electron "bottom". In front of these detectors there are coincidence counters and thin-plate spark-chambers (for clarity, all are omitted in Fig. 1).

iv) Two neutron detectors, called neutron "left" and neutron "right", with anticoincidence counters G_L and G_R in front of them to reject charged particles impinging on the "neutron" counters.

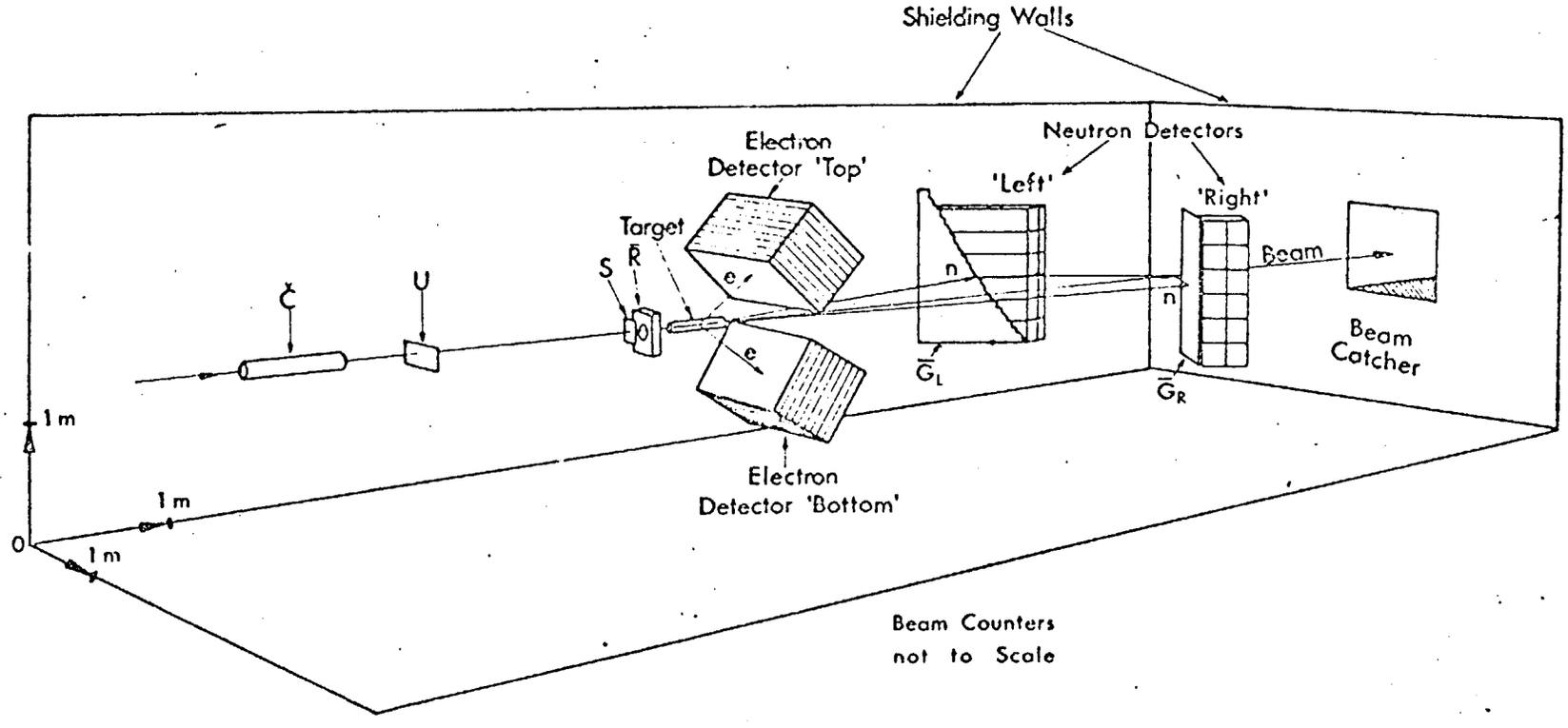
Shielding Walls
Neutron Detectors
Electron
Detector 'Top'
'Left'
'Right'
Target
S
R̄
C
U
e
n
n
Beam
Beam
Catcher
$\bar{G}_L$
$\bar{G}_R$
e
1 m
1 m
1 m
0
Electron
Detector 'Bottom'
Beam Counters
not to Scale

Fig. 1

As the reaction to be studied is

$$\pi^- + p \rightarrow n + M^0 \qquad M^0 \rightarrow e^+e^- \text{ or } \gamma\gamma \qquad (2)$$

it is clear that we need a large "neutron" detector and a large "electromagnetic shower" detector in order to measure with good acceptance all the particles that are present in the final state of reaction (2).

For the neutron in reaction (2), the neutron detector measures its time of flight t_n and its angle of emission Θ_n, thus allowing a determination of the missing mass, i.e. of the mass of the produced meson M^0. The mass resolution depends on the kinematical region in the plane (t_n, Θ_n) (see Fig. 2). It is ±4 MeV in the η-mass region, ±10 MeV in the ω-mass region and ±15 MeV in the φ-mass region. These mass resolutions were achieved using two identical neutron detectors, each having a sensitive surface and volume equal to 1.08 m^2 and 0.39 m^3, respectively.

2.1 The neutron detectors

A neutron detector is made of 12 elements of plastic scintillator, each having dimensions (100 × 18 × 18) cm^3, and each being viewed by two XP-1040 photomultipliers, one at either end (see Fig. 3 for details). The large volume of scintillator, in the particular geometrical arrangement chosen, allows a mean

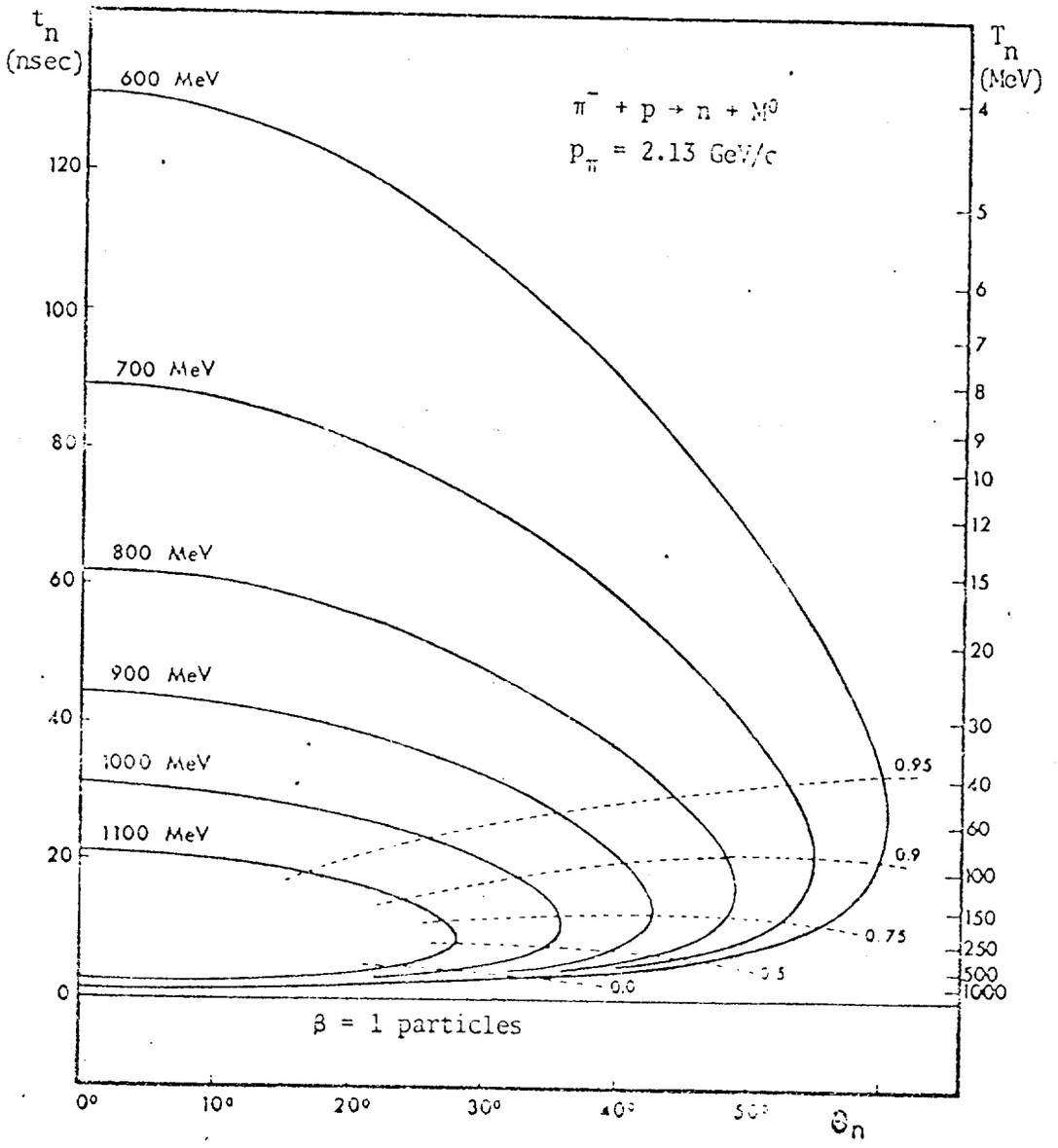

Fig. 2

detection efficiency of about 26% in the range (40-560) MeV neutron kinetic energy, for a laboratory solid angle of 0.14 sr at 4 m radial distance. An interesting feature of this instrument is the accuracy achieved in locating incident particles; this accuracy is ±1.4 cm for charged particles, and ±2.5 cm for neu-

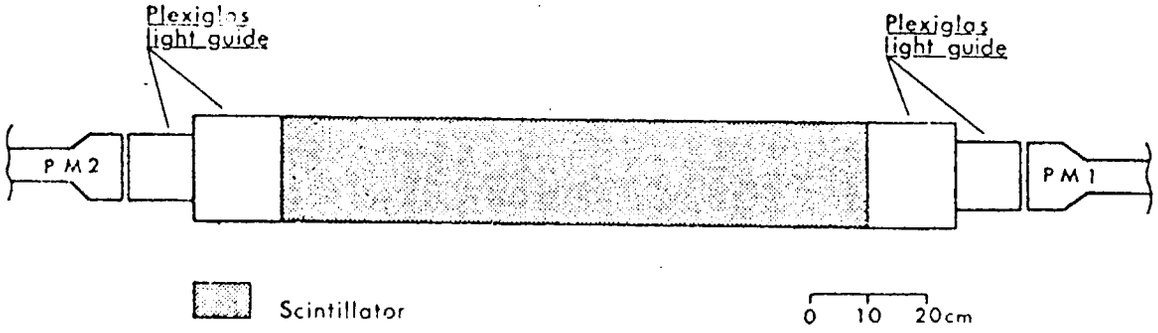
Plexiglas light guide
Plexiglas light guide
PM2
PM1
Scintillator
0 10 20cm

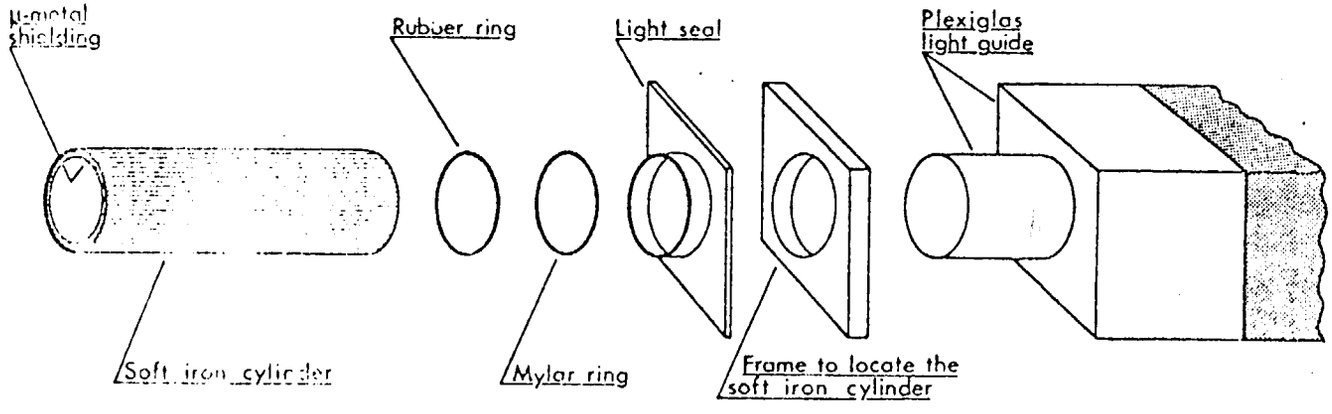
μ-metal shielding
Rubber ring
Light seal
Plexiglas light guide
Soft iron cylinder
Mylar ring
Frame to locate the soft iron cylinder

Fig. 3

trons. The accuracies achieved for the time-of-flight measurements are ±0.35 nsec for charged particles and ±0.7 nsec for neutrons. It is interesting to note that the accuracy in timing all elements of the two neutron detectors was ±0.1 nsec. An example of this time-equalization is shown in Fig. 4. In Fig. 4, t_1 is the

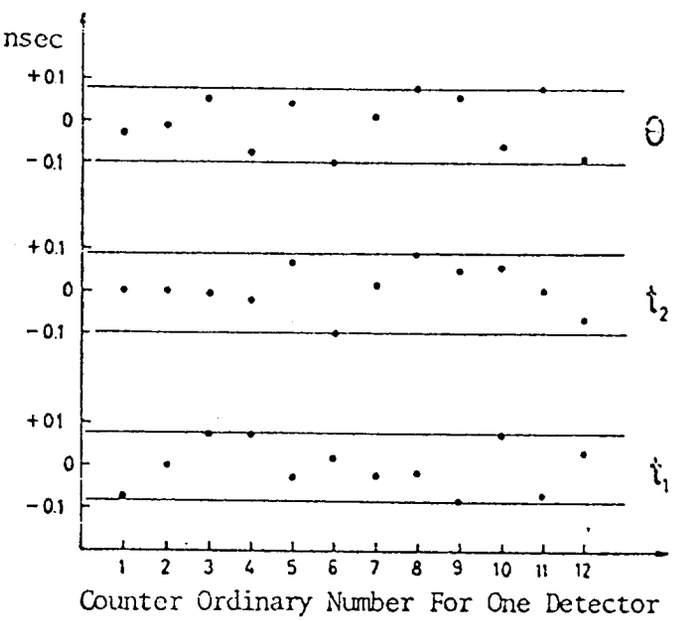

Fig. 4

time difference between the beam counter U and one of the two edges of the neutron counter; t_2 is that for the other edge; and θ is the difference between the two, obtained electronically*).

*) For more details on this instrument we refer the reader to Bollini et al.[1].

Typical data on position resolution and linearity of the neutron counters are shown in Figs. 5 and 6, respectively.

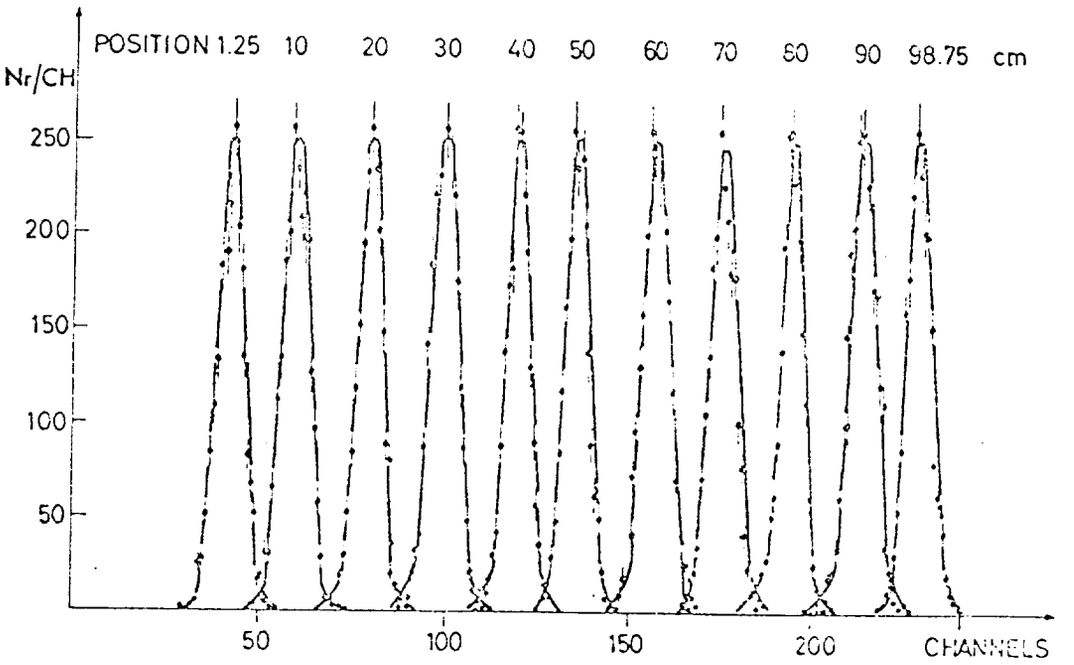

Fig. 5

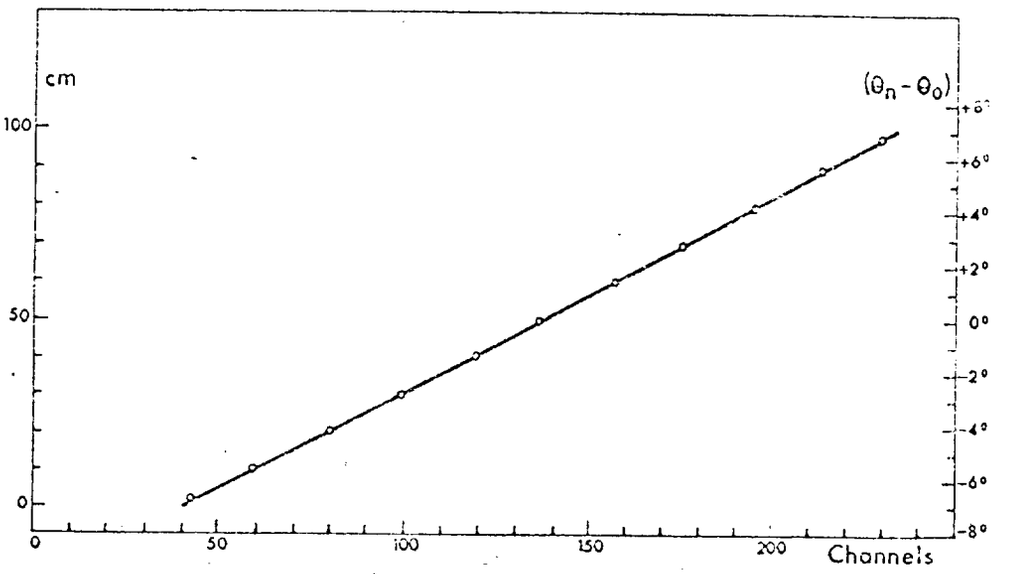

Fig. 6

In Fig. 5 the curves are labelled with the distance from the edge of the counter, and the spatial resolution for all positions in the counter is ±1.4 cm for charged particles.

In Fig. 6 the ordinate is the distance from one edge of the counter, and the abscissa is the channel number in which the peak corresponding to a certain position (as shown in Fig. 5) falls. The counter is seen to be linear. Notice that we have a total of 24 elements, and for all of them the above calibrations were repeated periodically in order to check that the apparatus worked correctly. For example, the neutron counter stability over a period of one week is shown in Fig. 7, where the time variation for θ, t_1, and t_2 signals is plotted for each element of the neutron counter. The time stability of the neutron detector is remarkably good.

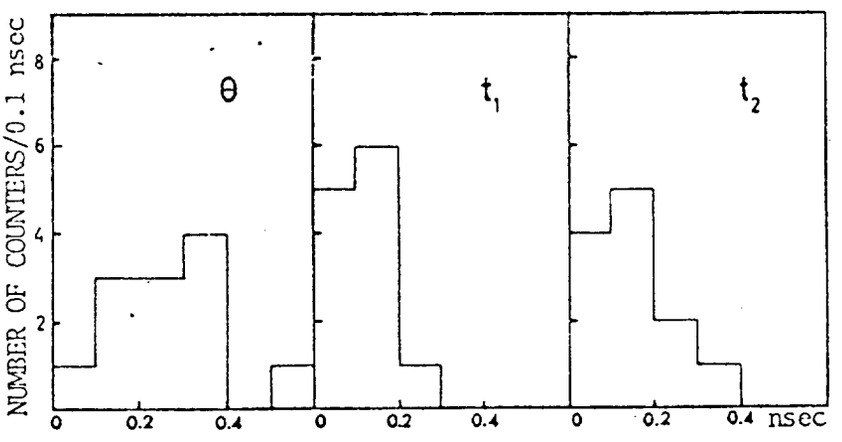

Fig. 7

2.2 The electromagnetic shower detectors

In Fig. 8 is shown a detailed drawing of the shower detectors. Each shower detector consists of nine elements, each one being made of a piece of lead followed by a two-gap spark chamber and a plastic scintillation counter. The first layer of lead is two radiation lengths thick; the other layers are one radiation length thick. The over-all thickness of the detector is half a metre. Before the first layer of lead there are two thin-plate spark chambers placed so as to ensure precise kinematical reconstruction of the events. Thus we could use a long H_2 target when looking for rare events, without losing accuracy in the missing-mass measure-

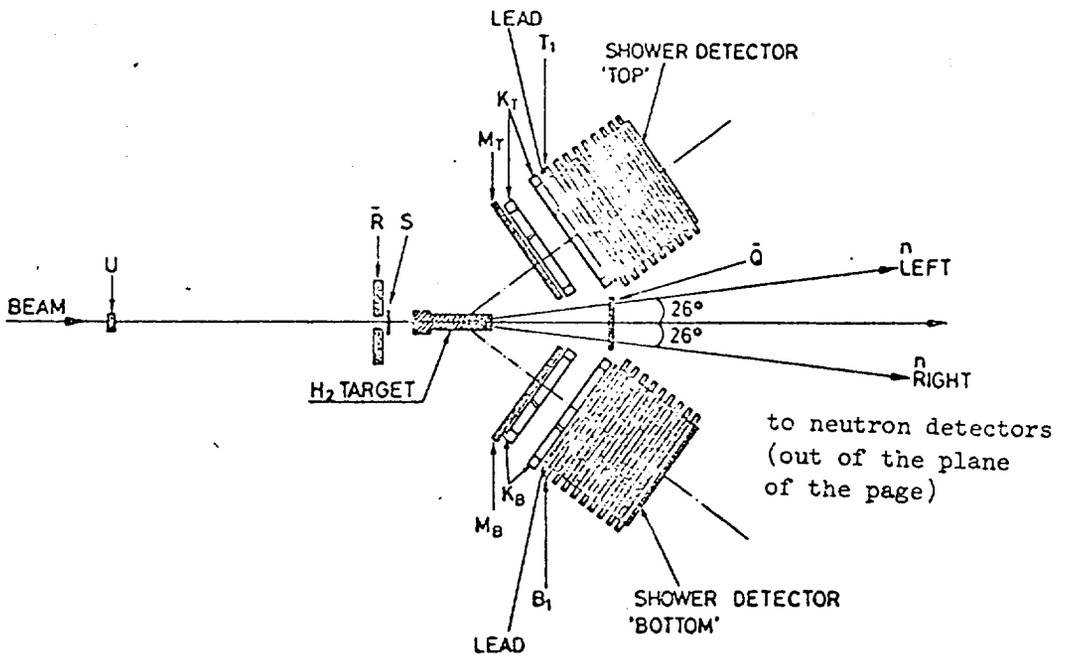

Fig. 8

ments from the neutrons. The two detectors may be rotated independently about a horizontal and a vertical axis through the H_2 target.

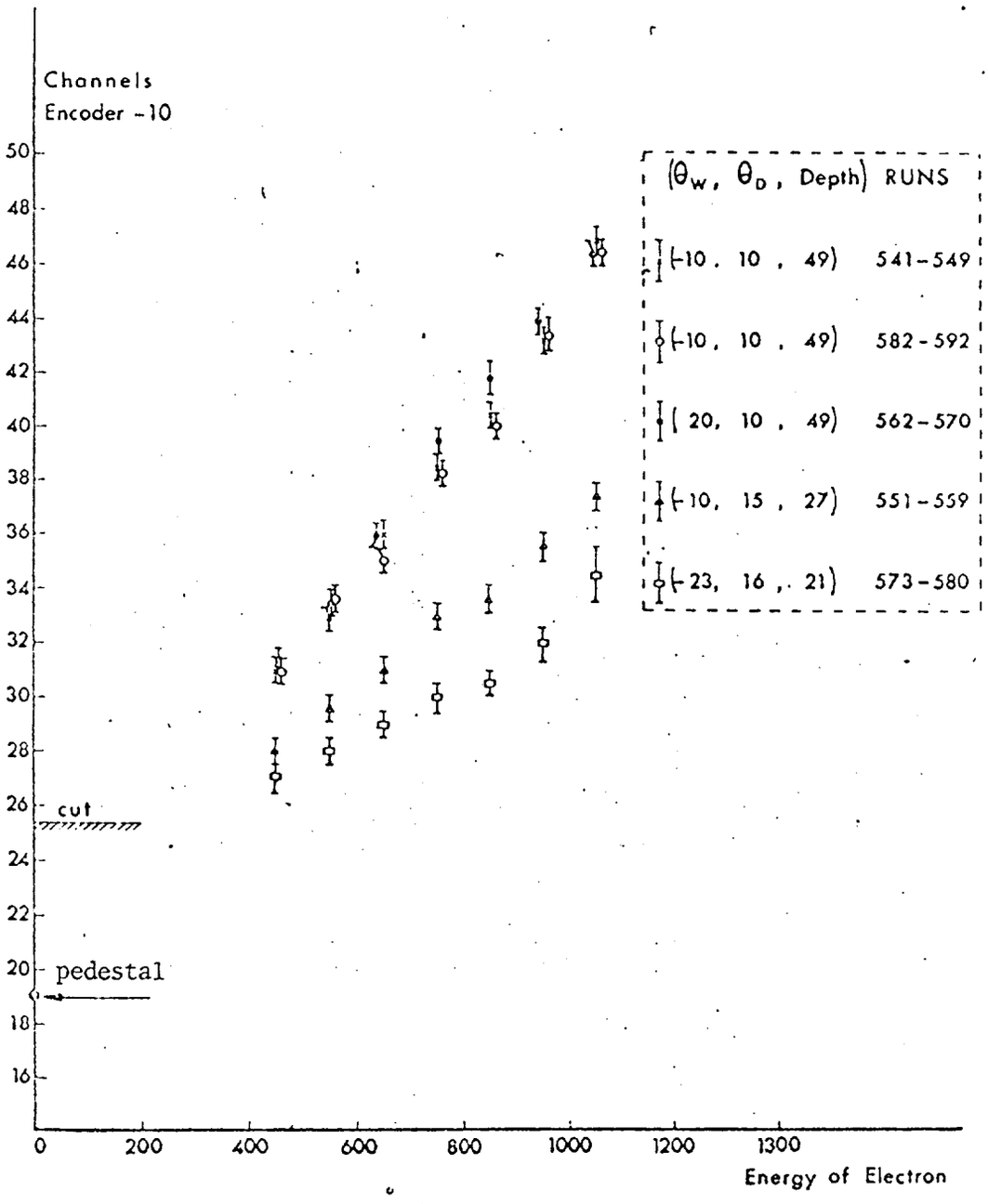

Fig. 9

Figure 9 shows a calibration of one of the two electron detectors. The response of the telescope is plotted as a function of the energy of the beam. We see that the instrument is linear. The three sets of points in the upper curve correspond to measurements made at different times (given by the run number) and to two different positions of the beam in the detector. Near the extremes of the detector the pulse height decreases, and we parametrize the calibrations according to the maximum depth of the detector available to the shower. The two lower curves are two of these edge-effect calibrations. During the calibrations, the detectors were rotated to many positions and calibrated as a function of depth and energy in order to allow the calculation of the total efficiency for any event configuration. For fixed depth we see that the fluctuations are small; in any case we calibrate the system very often in order to be sure that when we say we have an electron it is indeed an electron and not a pion.

Figure 10a shows a complete efficiency calibration at fixed energy. The purpose of this figure is to show that the electromagnetic shower detectors "top" and "bottom" behave in a completely identical way. The open circles refer to the bottom detector and the full circles to the top detector. The electron energy for these two sets of points is 1050 MeV. Figure 10b shows a family of curves

corresponding to 170 calibration points taken at different energies, from 1.05 GeV down to 0.45 GeV.

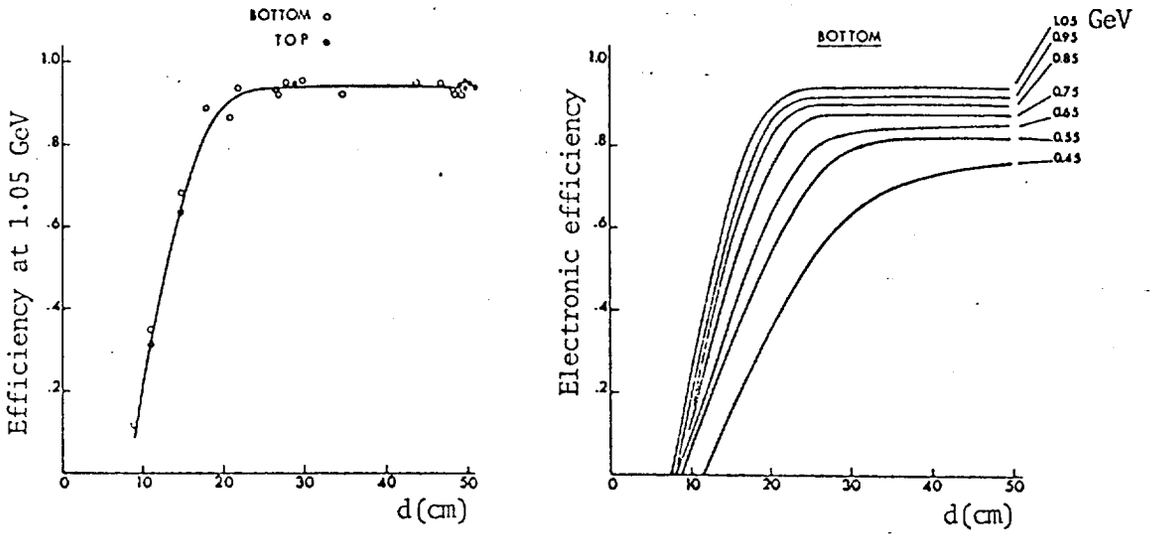

(a) (b)

Fig. 10

Table 1 summarizes the efficiencies of our detectors. From as low as 400 MeV up to 1100 MeV we can reject pions with a power of 3×10^{-4}. For each particle and each momentum there are three numbers: the electronic efficiency; the picture analysis efficiency; and their product, the over-all efficiency.

As I have said, the electromagnetic detectors consist of counters and spark chambers, so we have an electronic rejection in the trigger; then, once we have taken the pictures, we can make further rejection in the picture analysis. The latter is very important because it allows us to eliminate the charge exchange of pions, which is the greatest source of trouble when you want to distinguish a

Table 1

Efficiency in detector "bottom"

Momentum in MeV/c	Particle	Electronic efficiency	Picture analysis efficiency	Over-all efficiency
400	e	(77.5 ± 2.2)%	(89.0 ± 2.2)%	(69.0 ± 2.6)%
	π	(6.3 ± 0.2)%	(0.43 ± 0.2)%	$(2.7 \pm 1.6) \times 10^{-4}$
1100	e	(94.0 ± 1.5)%	(88.0 ± 2.0)%	(83.0 ± 2.3)%
	π	(17.6 ± 0.6)%	(0.16 ± 0.16)%	$(2.8 \pm 2.8) \times 10^{-4}$

pion from an electron. From 400 to 1100 MeV, the rejection power of the telescope against pions is practically the same and the efficiency for electron detection is very good, between 70% and 80%. Conclusion: we have two telescopes and in each telescope we have 3×10^{-4} rejection against pions. This squared is about 10^{-7}. This means that we can reject charged $\pi\pi$ pairs and charged multi-pion events with this power. It is this rejection power that allows us to look at rare events such as (e^+e^-) decay of strongly interacting particles.

3. SOME RELEVANT DETAILS

Table 2 summarizes the most relevant parameters of the actual experiment for ω and ϕ decays into e^+e^-. The meaning of the symbols is the following:

p_π	is the primary pion momentum. It has been chosen at the maximum of the production cross-section.
$\Theta^{\text{neutron}}_{\text{lab.}}$	is the angular range covered by the neutron detectors in the lab. system.
$\Theta^{\text{neutron}}_{\text{centre of mass}}$	is the corresponding value in the centre-of-mass system.
T_n	is the range of neutron kinetic energies accepted in the above angular range. It follows the corresponding range of neutron time-of-flight t_n.
q^2	is the range of four-momentum transfer.
ΔM	is the mass uncertainty.
$\Theta^{\text{vector-meson}}_{\text{lab.}}$	is the angular range of vector meson production.
Θ^D	is the angular position of the electron detectors in the vertical plane containing the beam.
T_1 and B_1	are the thresholds of the first counters in the shower detectors, i.e. after two radiation lengths in lead.

Table 2

Vector meson decays → e^+e^-

	ω	φ
p_π	1.67 GeV/c	1.93 GeV/c
θ neutron lab. (counter)	31° to 45°	19° to 33°
θ neutron centre of mass	165° to 94°	160 to 70
T_n	42 to 430 MeV	95 to 560 MeV
t_n	46 to 18 nsec	32 to 17 nsec
q^2	0.08 to 0.08 $(GeV/c)^2$	0.18 to 1.1 $(GeV/c)^2$
ΔM	±10 MeV	±15 MeV
$\theta_{lab.}$ vector-meson	6° to 32°	5° to 25°
θ^D	32°	36°
$T_1 = B_1$ threshold	$1.7 \times \left(\frac{dE}{dx}\right)_{min}$	
$\Sigma T = \Sigma B$ threshold	150 MeV	
$\Sigma\Sigma$ threshold	700 MeV	

ΣT and ΣB are the thresholds of the two electromagnetic shower detectors "top" and "bottom". These thresholds were fixed at a very low value of 150 MeV incident electromagnetic energy in order to have high efficiency in the detection of electromagnetic showers.

$\Sigma\Sigma = \Sigma T + \Sigma B$ is the total electromagnetic energy release in "top" plus "bottom". We trigger every time that the total energy is greater than 700 MeV; again this choice of low threshold is taken in order to have good detection efficiency for electromagnetic showers originated either by electrons or by photons.

Another important point worth mentioning is the way in which we reject $\gamma\gamma$ events. In the description of the electromagnetic shower detectors, it was pointed out that the rejection power against charged $\pi\pi$ pairs was 10^{-7}. But in $(\pi^- p)$ interactions, two or more π^0's can be produced: the π^0's decay into γ's, which then materialize in the target or in the plastic scintillator before the thin-plate spark chambers, thus producing electron-positron pairs which can simulate a genuine $e^{\pm}$ from vector meson decay. It is possible to recognize

most of these γ-produced "fake $e^{\pm}$" because they are really "electron-positron pairs" whose opening becomes sufficiently large by multiple scattering in the traversal of the material that is in front of the kinematic spark chambers. The distribution of the distance between two tracks of a pair is shown in Fig. 11. The wide part of the spectrum is that expected from multiple scattering (this point will be discussed further in the section on the X^0). The peak at zero is clearly due to genuine single $e^{\pm}$ and <u>not</u> to (e^+e^-) pairs that look like a single track. In fact from the measured distribution (shown in Fig. 11), the number of "fake $e^{\pm}$" present in the peak is expected to be ~ 2.

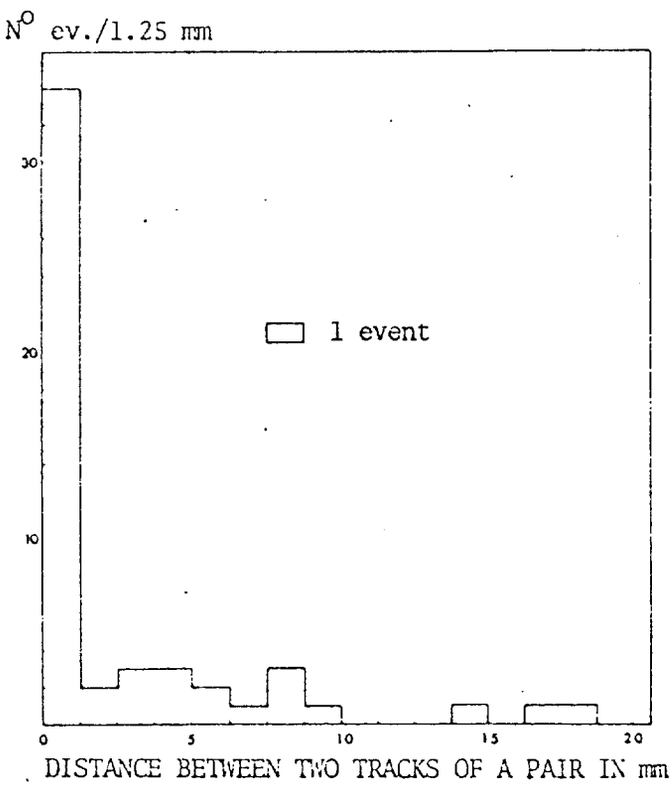

Fig. 11

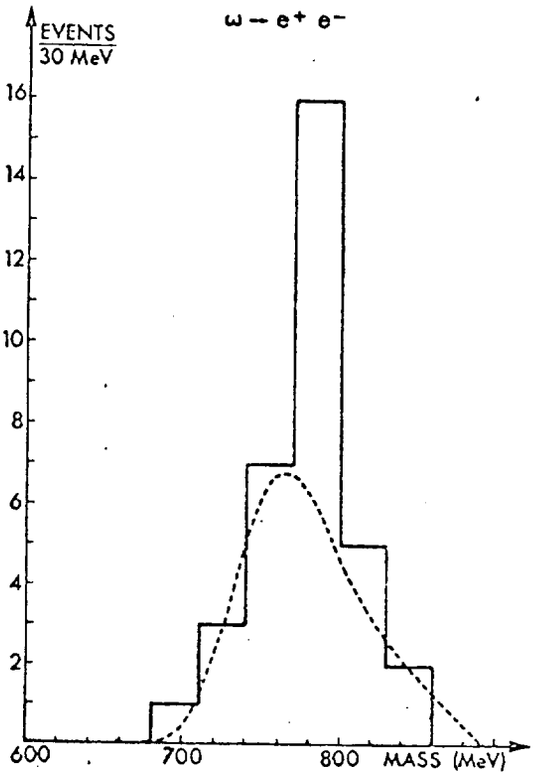

Fig. 12

If we now plot the mass distribution of the events in the peak of Fig. 11, we obtain the distribution shown in Fig. 12.

Notice that this result represents the first successful attempt to resolve the ω-peak from the ρ. As mentioned in the introduction, the experimental conditions were chosen in such a way as to minimize the amount of observable ρ's. In fact, the broken curve is the expected ρ-mass distribution calculated from the known production and decay angular distribution combined with the experimental acceptance.

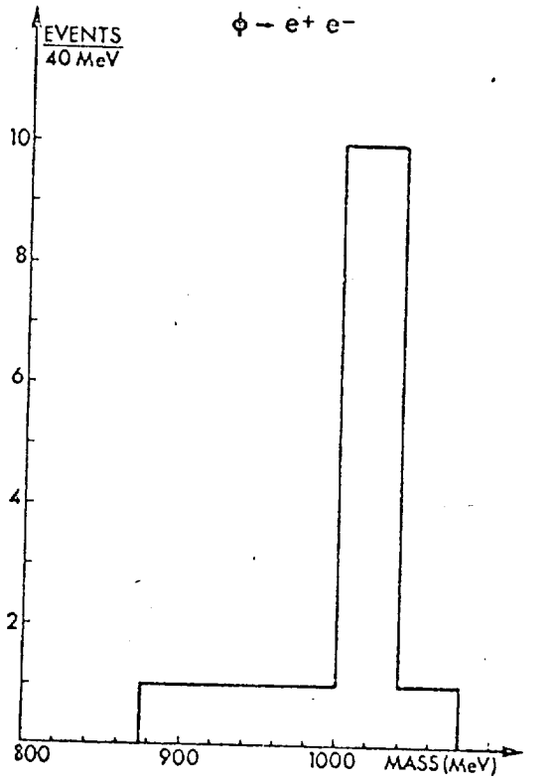

Fig. 13

Repeating the same type of analysis for the ψ-case gave the mass distribution shown in Fig. 13. In the ϕ-mass region there is a total of ten events minus one background event. To have a small background was an essential feature of the experiment, the limitation in the number of observed $\phi \to e^+e^-$ being due to the available machine time. Notice the difference between the distribution shown in Fig. 13 and that of the previous one shown in Fig. 12. The background below the ϕ-peak is flat because there is no ρ-like object in the ϕ-mass region. In conclusion, a total of nine events of unambiguously identified $\phi \to e^+e^-$ decays were observed.

4. RESULTS ON THE e^+e^- DECAYS OF ω AND ϕ

Table 3 below summarizes the results obtained on the e^+e^- decays.

Table 3

	$\omega \to e^+e^-$	$\phi \to e^+e^-$
$\sigma(\pi^- p \to nM^0) \hookrightarrow e^+e^-$	$(67 \pm 25) \times 10^{-33}$ cm^2	$(18.4 \pm 6.9) \times 10^{-33}$ cm^2
$\sigma(\pi^- p \to nM^0) \hookrightarrow$ all	$(1.67 \pm 0.07) \times 10^{-27}$ cm^2	$(30 \pm 6) \times 10^{-30}$ cm^2
$\frac{\Gamma(M^0 \to e^+e^-)}{\Gamma(M^0 \to \text{all})}$	$(4.0 \pm 1.5) \times 10^{-5}$	$(6.1 \pm 2.6) \times 10^{-4}$
$\Gamma(M^0 \to \text{all})$	(12.2 ± 1.3) MeV	(3.4 ± 0.8) MeV
$\Gamma(M^0 \to e^+e^-)$	(0.49 ± 0.19) keV	(2.1 ± 0.9) keV

The first entry is the direct experimental result obtained. Below there is the ω production cross-section, which is well known; these two numbers then give the branching ratio, which together with the total width of the ω taken from the Rosenfeld Tables[2] give the partial width in the last entry. In the case of the ϕ, the production cross-section is much lower and is not so well known as that of the ω. In fact, we have measured a point[3] in the cross-section, because when we started the experiment the ϕ production had not been observed in pion-nucleon

interactions[4]. The energy at which we measured the ϕ production cross-section[3] is slightly higher than that at which we stayed. We were in fact looking for a maximum value in the cross-section, when a bubble chamber group[5] published a paper in which the maximum seemed to be 150 MeV lower; so we decided to stay lower. Notice that our value of the ϕ production cross-section is in very good agreement with the bubble chamber data[5]. Again the total width is taken from the Rosenfeld Tables[2] in order to derive the partial width.

5. COMPARISON WITH THEORY -- THE (ω-ϕ) MIXING ANGLE

The interest in the decay of the vector meson into e^+e^- lies not only in the fact that these decays had to be seen, but because to look for these decay modes allows one to check a key point of SU(3) symmetry, namely the (ω-ϕ) mixing hypothesis.

As you know, a remarkable feature of particle physics is the existence of SU(3) [6,7]; what is even more remarkable is the regularity of SU(3) breaking, postulated by Gell-Mann[6] and Okubo[8] to be as simple as a coherent superposition of an SU(3) singlet and the 8^{th} component of an SU(3) octet, and found to be in agreement with all known SU(3) multiplets except the vector meson octet. This failure was turned into a success by Sakurai[9] who, following Gell-Mann[6], put forward the hypothesis that the reason for the non-validity of the

Gell-Mann - Okubo mass formula was the fact that the physically observed ω and ϕ mesons are a mixture of a pure SU(3) singlet ω_1 and of a pure 8^{th} component of an SU(3) octet ω_8. Moreover, the ω-ϕ mixing mechanism provided a simple dynamical mechanism to explain the above-mentioned regularity of SU(3) breaking[10].

The (ω-ϕ) mixing started to be described by a mixing angle θ. By now there are four mixing angles quoted in the literature[9-16]: the original θ, then θ_Y, θ_N, and finally the generalized mixing angle θ_G.

We shall now try to review the origin of all these mixing angles. The starting point is: two particles with identical quantum numbers (J^{PC}, I, Y) such as ω_8 and ω_1 will convert into each other

$$\omega_8 \rightleftarrows \omega_1 \tag{3}$$

because process (3) does not violate any conservation law but that of SU(3) symmetry, which is broken by the moderately strong interactions. As it is impossible to switch off these interactions, process (3) will go.

When two particle states can convert into each other, as in process (3), the inverse propagator that describes the mixed system can be shown to have the familiar form

$$D = AK^2 + BM^2 \ , \tag{4}$$

where A and B are 2 × 2 matrices (if we want to describe mixing between two particles only); K is the quadrimomentum; and M is the mass of the two states. Let D_0, A_0, and B_0 be the quantities defined above before the mixing starts. Without mixing the two matrices, A_0 and B_0 are diagonal, i.e.:

$$A_0 = \begin{pmatrix} 1 & 0 \\ 0 & 1 \end{pmatrix}; \qquad B_0 = \begin{pmatrix} \beta_1 & 0 \\ 0 & \beta_2 \end{pmatrix},$$

and the inverse propagator

$$D_0 = A_0K^2 + B_0M^2 \tag{S}$$

gives the two propagators of the two unmixed states, each having momentum K and masses β_1M^2 and β_2M^2 (β_1 and β_2 are just numerical coefficients). The effect of mixing can be of two types. These two ways of treating the mixing between two particles have been discussed first by Coleman and Schnitzer[13] (CS) and later by Kroll, Lee and Zumino[14] (KLZ), who particularly emphasized the need of having two mixing angles.

Mass mixing

Here it is supposed that the effect of mixing [process (3)] is that of destroying the diagonality of the matrix B_0, which becomes $B = B_0 + \delta B$, without disturbing the matrix A_0.

The problem is to diagonalize B and hence D without destroying the diagonality of A_0. It is well known that in order to achieve this, the matrix that is needed can be an orthonormal matrix. As the elements of a 2 × 2 matrix are four, and the orthonormality conditions are three, all the mixing can be described using a single parameter: the mixing angle Θ, which is the angle first introduced by Sakurai[9]. The left side of Fig. 14 shows a synthesis of the above chain of arguments.

Current mixing

Here it is assumed that the effect of mixing is to destroy the diagonality of A_0, leaving B_0 diagonal. The problem is now to diagonalize $A = A_0 + \delta A$, without destroying the diagonality of B_0. Notice that B_0 is diagonal but (unlike A_0) not unit. In order to diagonalize A without destroying the diagonality of the non-unit B_0, a 2 × 2 matrix, without orthonormality conditions, is required. The mixing must therefore be described using four parameters, which can be expressed in terms of two coupling constants g_Y and g_N, and of two mixing angles Θ_Y and Θ_N (here we use the same notation as KLZ). However, because of T, A and B_0 are symmetric matrices; this gives one condition for the four free parameters. This condition can be used in order to establish a relation between the two mixing angles Θ_Y and Θ_N, i.e.

$(\omega - \varphi)$ MIXING

$$\boxed{D = AK^2 + BM^2}$$

WITHOUT MIXING: $A_0 = \begin{pmatrix} 1 & 0 \\ 0 & 1 \end{pmatrix}$; $B_0 = \begin{pmatrix} \beta_1 & 0 \\ 0 & \beta_2 \end{pmatrix}$

EFFECT OF MIXING:

i) MASS-MIXING

↓

DESTROY DIAGONALITY OF

B_0

↓

PROBLEM: DIAGONALIZE

$B = B_0 + \delta B$

WITHOUT DESTROYING DIAGONALITY OF

$A_0 = \begin{pmatrix} 1 & 0 \\ 0 & 1 \end{pmatrix}$

↓

MATRIX NEEDED:

$\begin{pmatrix} \alpha & \beta \\ \gamma & \delta \end{pmatrix}$ WITH $\left| \begin{array}{l} \alpha^2+\beta^2=1 \\ \gamma^2+\delta^2=1 \\ \alpha\gamma+\beta\delta=0 \end{array} \right|$ ORTHO-NORMALITY CONDITIONS

4 PARAMETERS − 3 CONDITIONS

↓

ONLY ONE PARAMETER

θ

ii) CURRENT-MIXING

↓

DESTROY DIAGONALITY OF

A_0

↓

PROBLEM: DIAGONALIZE

$A = A_0 + \delta A$

WITHOUT DESTROYING DIAGONALITY OF

$B_0 = \begin{pmatrix} \beta_1 & 0 \\ 0 & \beta_2 \end{pmatrix}$

↓

MATRIX NEEDED:

$\begin{pmatrix} \alpha & \beta \\ \gamma & \delta \end{pmatrix}$ NO ORTHO-NORMALITY CONDITIONS

4 PARAMETERS:

| 2 COUPLING CONSTANTS: g_Y , g_N

| 2 ANGLES: θ_Y, θ_N

CORRELATED

↓

$\frac{m_\omega}{m_\varphi} \tan\theta_Y = \frac{m_\varphi}{m_\omega} \tan\theta_N = \tan\theta_G$

COMPARE

Fig. 14

$$\frac{\tan \Theta_Y}{\tan \Theta_N} = \frac{m_\phi^2}{m_\omega}$$

first derived by KLZ. This relation can be rewritten as

$$\frac{m_\omega}{m_\phi} \tan \Theta_Y = \frac{m_\phi}{m_\omega} \tan \Theta_N = \tan \Theta_G \qquad (6)$$

thus allowing the mixture to be expressed in terms of the "generalized" mixing angle Θ_G [16]. The right-hand side of Fig. 14 illustrates the above chain of arguments.

Why are there all these complications?

After the introduction of the $(\omega_8-\omega_1)$ mixing hypothesis by Sakurai[9], CS[13] emphasized that the Sakurai-type of mixing, called by them "particle mixing" and by KLZ[14] "mass-mixing", was not adequate enough to describe mixing between "vector particles". This is because vector particles are believed to be associated with conserved quantities, and "mass mixing" is incompatible with this requirement, as can be easily shown with the following example. Suppose that the inverse propagator D describes the isoscalar form factor of the nucleon*) and that we choose the "mass mixing" model. After mixing, D_0 becomes D:

$$D_0 = A_0K^2 + B_0M^2 \xrightarrow{\text{mixing}} D = A_0K^2 + (B_0 + \delta B)M^2.$$

At $K^2 = 0$, $D_0 \neq D$. But the value of D_0 and D at $K^2 = 0$ is related to the nuclear isoscalar electric charge (i.e. electric charge of the proton divided by two). The effect of "mass mixing" is to change the value of the nuclear isoscalar electric charge and this is unacceptable.

If we choose "current mixing" we have

$$D_0 = A_0K^2 + B_0M^2 \xrightarrow{\text{mixing}} D = (A_0 + \delta A)K^2 + B_0M^2 ,$$

---

*) Pole dominance is of course assumed.

and at $K^2 = 0$ it is $D_0 = D$. This is the reason why "current mixing" is believed to be more adequate for the description of the mixing between vector particles.

It is interesting to notice[13] that if the force mixing the particles is truly weak, "mass mixing" and "current mixing" are indistinguishable [as in the case of the $(K^0-\bar{K}^0)$ mixing which produces the physically observed states K_L^0 and K_S^0; but here the transition $K^0 \rightleftarrows \bar{K}^0$ is a second-order weak interaction]. Notice that in the above models of mixing it has always been assumed that the mixing alters only the propagators and not the vertex functions. Notice also that both "current mixing" and "mass mixing" are compatible with the transversality conditions for the source of the vector mesons[14], i.e. the currents to which they are coupled are conserved currents.

All these conditions still do not make known the value of the ω-ϕ mixing. To attain this a detailed model is necessary, and many of these exist in the literature. They are all reported in Fig. 15. Notice that the prediction of the current mixing model (CMM) of Kroll, Lee and Zumino[14] differs from that of Oakes - Sakurai[16] because of the use of slightly different mass values for ω and ϕ mesons. The difference between Das - Mathur - Okubo[15] and Oakes - Sakurai[16] is due to second-order SU(3) breaking effects. It should be mentioned that what appears in Fig. 15 is the generalized mixing angle θ_G. In fact, according to

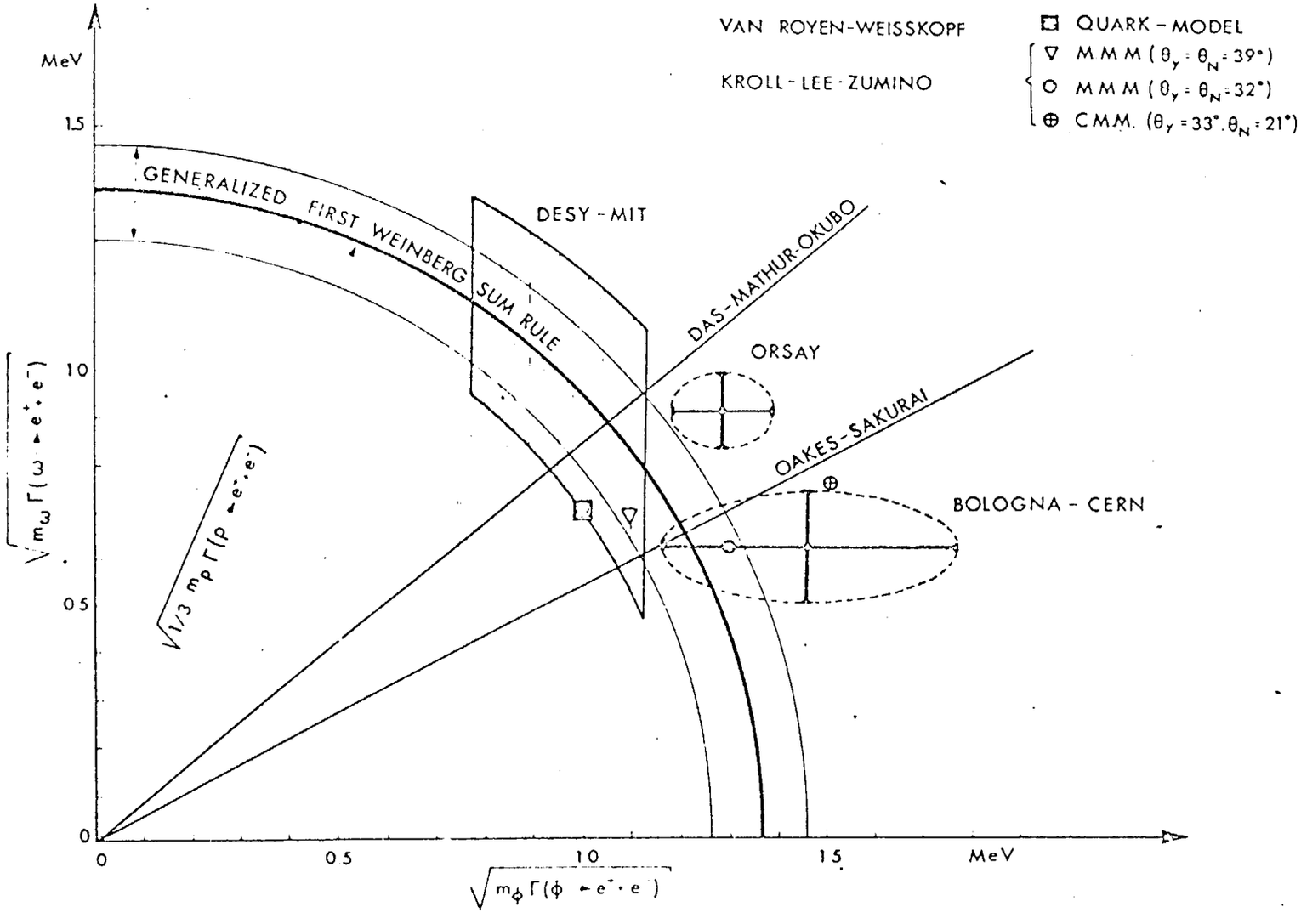
VAN ROYEN-WEISSKOPF
KROLL-LEE-ZUMINO
QUARK-MODEL
MMM ($\theta_V = \theta_N = 39°$)
MMM ($\theta_V = \theta_N = 32°$)
CMM. ($\theta_V = 33°, \theta_N = 21°$)
GENERALIZED FIRST WEINBERG SUM RULE
DESY-MIT
DAS-MATHUR-OKUBO
ORSAY
OAKES-SAKURAI
BOLOGNA-CERN
MeV
1.5
1.0
0.5
0
0.5
1.0
1.5
MeV
$\sqrt{m_\omega \Gamma(\omega \to e^+ e^-)}$
$\sqrt{1/3\, m_\rho \Gamma(\rho \to e^+ e^-)}$
$\sqrt{m_\phi \Gamma(\phi \to e^+ e^-)}$

Fig. 15

KLZ[16], the following relation holds:

$$\frac{\sqrt{m_\omega \Gamma(\omega \to e^+e^-)}}{\sqrt{m_\phi \Gamma(\phi \to e^+e^-)}} = \frac{m_\omega}{m_\phi} \tan \theta_Y = \tan \theta_G \ .$$

The radius of the circle corresponds to the quantity $1/3\ m_\rho\ \Gamma(\rho \to e^+e^-)$ with its experimental uncertainty. The relation between $m_\omega\ \Gamma(\omega \to e^+e^-)$, $m_\phi\ \Gamma(\phi \to e^+e^-)$, and $m_\rho\ \Gamma(\rho \to e^+e^-)$ is obtained by the generalization of the first Weinberg Spectral Function Sum Rule (WSFSR)[17], due to Das-Mathur-Okubo[15] and Oakes-Sakurai[16], who derived the relation

$$\frac{1}{3}\, m_\rho\, \Gamma(\rho \to e^+e^-) = m_\omega\, \Gamma(\omega \to e^+e^-) + m_\phi\, \Gamma(\phi \to e^+e^-$$

among particles carrying different isospin. It is remarkable that the quark model predictions of Van Royen and Weisskopf[18] numerically satisfy the generalized first WSFSR.

The results plotted correspond to the Bologna-CERN data[19] plus those obtained by Ting at DESY[20] and by the (e^+e^-) colliding beams experiments done at ORSAY[21].

The CERN-Bologna result[19] is the first measurement of the $(\omega$-$\phi)$ mixing angle, the value of θ_G being:

$$\theta_G = (23^{+7}_{-5})^\circ \ ,$$

in excellent agreement with the current mixing model of KLZ[14] and of Oakes and Sakurai[16].

The effect of $(\omega-\rho)$ interference has been estimated[22], the result being a variation of $(\pm 3)^\circ$ for complete constructive or destructive interference, respectively. It should be noticed that in the OPE model the $(\omega-\rho)$ interference is exactly zero.

In conclusion, the results obtained by the Bologna-CERN group in the field of (e^+e^-) decays of vector mesons made it possible to reach the following conclusions:

i) The general idea of $(\omega-\phi)$ mixing is confirmed.

ii) The generalized first Weinberg Spectral Function Sum Rule (saturated using only ρ, ω, ϕ) is valid within 30% over-all experimental uncertainty.

iii) There is no evidence for the coupling of the electromagnetic field to an SU(3) singlet.

iv) The old A quantum number[23] is not a good quantum number.

v) The fact that we observe these decays is direct evidence that the J^{PC} quantum numbers of the ω and ϕ are indeed 1^{--}.

6. $X^0 \to \gamma\gamma$

Now we go to $X^0 \to \gamma\gamma$. Here we have a different problem: how do we see $\gamma\gamma$ events? Remember that we reconstruct the events in the thin-plate kinematic chambers. The method is very simple: these events come in as a background in our $\phi \to e^+e^-$ experiment, and the γ-rays materialize in the target walls or in the plastic scintillation counters which are placed in front of the kinematic chambers. The efficiency for this conversion is about 7%, which is the reason why we do not have many X^0 events.

Figure 16 shows the losses that we had. We say that we do observe $X^0 \to \gamma\gamma$

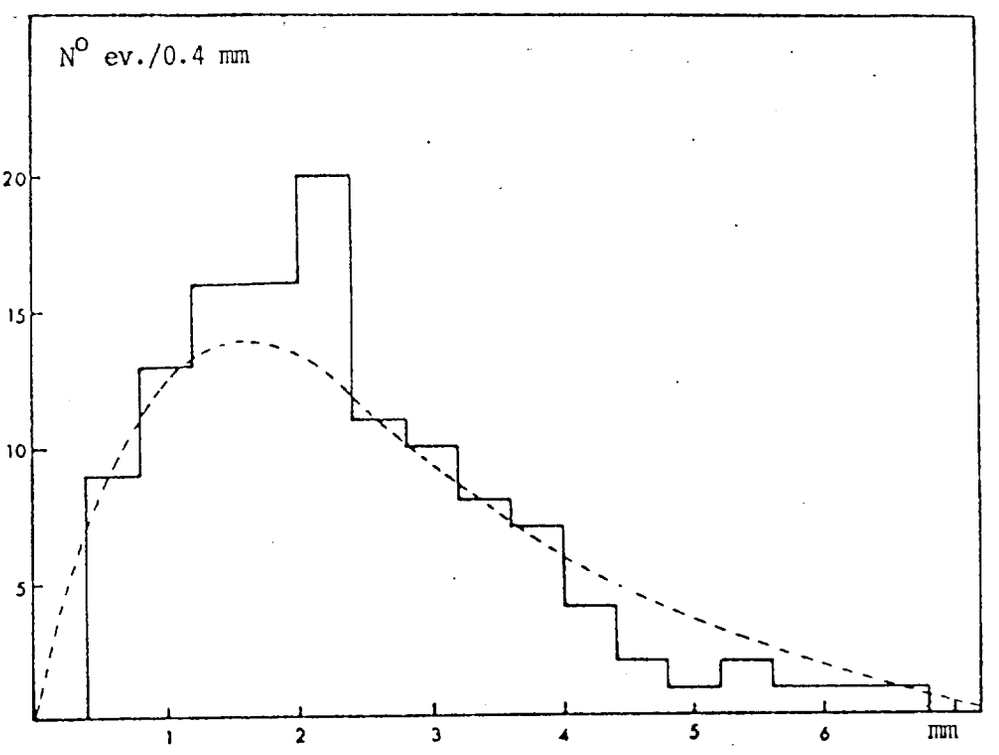

Fig. 16

if we see that the photons produce two very narrow e^+e^- pairs, one in each detector. The dotted line is the expected opening distribution of the pairs by multiple scattering. The histogram is a distribution taken from a subset of our triggers in which there was a pion in one chamber and a gamma in the other. Events which fall in the bottom bin look like a single track and so are lost. This loss is small, but has been taken into account.

Figure 17a shows the mass distribution of events which we believe to be genuine $X^0 \to \gamma\gamma$ events. In fact the events of this set satisfy the kinematic tests and the pictures do not contain anything but the two γ's.

Figure 17b shows the mass distribution of those events in which there was either an extra shower or missing particles. This gives an idea of the background shape.

How do we normalize the dotted background line in Fig. 17a? We do a Monte Carlo calculation and argue as follows.

We have $\pi^- p \to \pi^0\pi^0$ which also looks like

$n\pi^0\gamma$ when one γ is lost, or like

$n\gamma\gamma$ when two γ's are lost outside the acceptance of the detector.

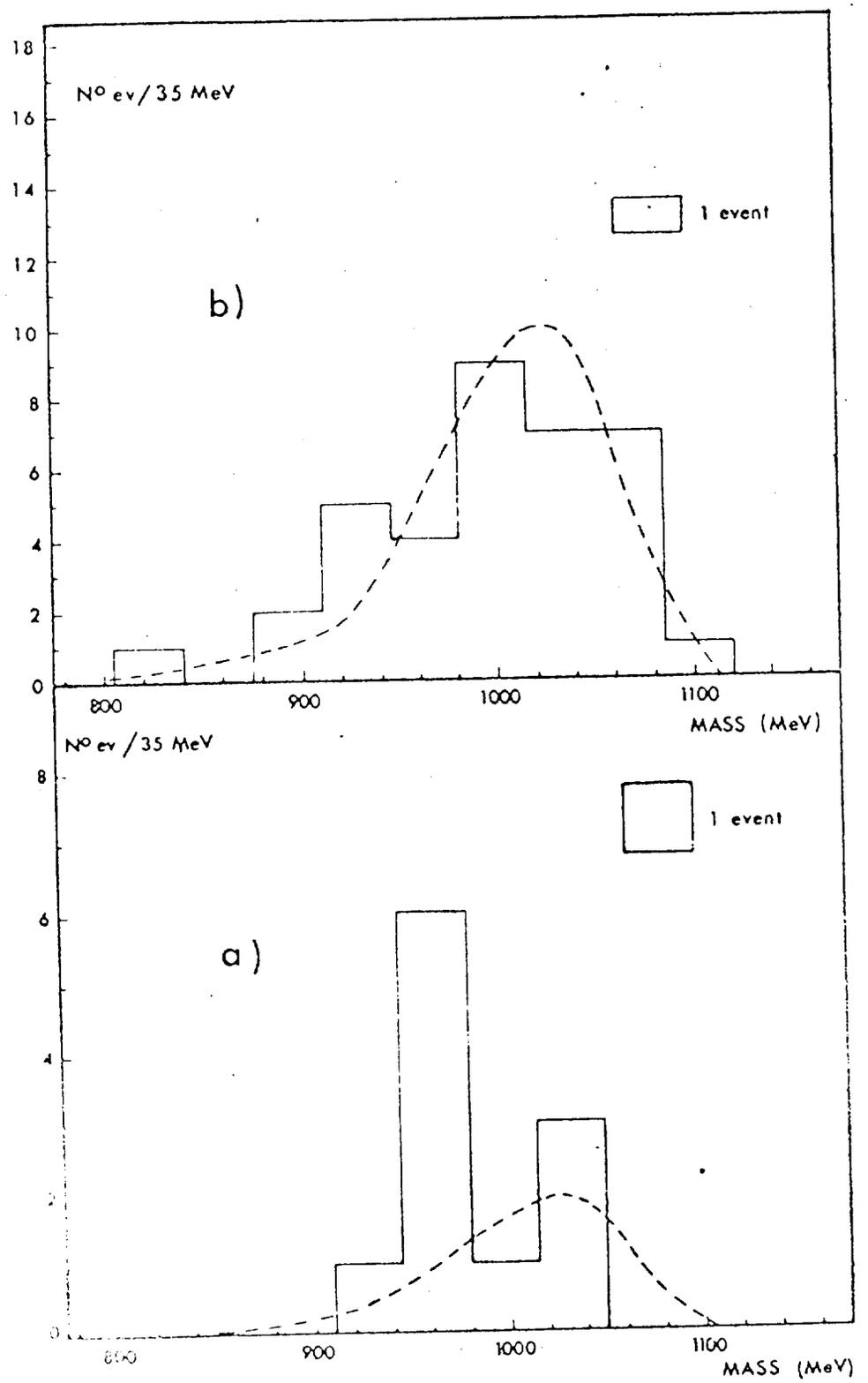

Fig. 17

Thus a $2\pi^0$ event can have 1γ, 2γ or 3γ observed in the electromagnetic detectors. By making a comparison of the numbers of events having 1γ, 2γ, or 3γ, with the numbers expected from Monte Carlo calculations, we can say how many of the $\gamma\gamma$ events were really $\pi^0\pi^0$ events. The result is extremely encouraging, and we predict that the number of events of this type should be very small; it should be about two. So below the peak we expect one background event. This agrees very nicely with what we see. All we claim here is having seen five genuine $\gamma\gamma$ events in the mass region (962 ± 17) MeV [24].

The probability that the peak is a statistical fluctuation of the background is less than 1%.

The most likely interpretation of the observed peak is the decay of the X^0 meson into 2γ *). This rules out $J^P = 1^\pm$ and provides direct evidence in support of the $J^{PC} = 0^{-+}$ assignment to the X^0 quantum numbers.

---

*) We know that in this mass region there are the δ and the H. But the δ needs confirmation, whilst the H seems dead. The X^0 is at present the best-established meson in this mass range. This is why we ignore possible contributions from other objects.

The determination of the branching ratio BR = $\Gamma(X^0 \to 2\gamma)/\Gamma(X^0 \to \text{total})$ is relevant to the understanding of the large $\gamma\gamma$ decay mode[25] of the η meson in connection with the problem of the X^0 being a member of the 0^- nonet. In order to estimate BR it is necessary to calculate the acceptance of our apparatus for $\gamma\gamma$ events. This has been done by Monte Carlo calculation, using the data of Abolins et al.[26] on the X^0 production angular distribution at the same incident pion energy.

The following value is found for the cross-section:

$$\sigma(\pi^- + p \to n + X^0 \hookrightarrow 2\gamma) = (8.8^{+5.1}_{-4.0}) \times 10^{-30} \text{ cm}^2 .$$

Using the known total production cross-section[26]:

$$\sigma(\pi^- + p \to n + X^0) = (0.16 \pm 0.05) \times 10^{-27} \text{ cm}^2 ,$$

the following value for the branching ratio is obtained:

$$BR = \frac{\Gamma(X^0 \to 2\gamma)}{\Gamma(X^0 \to \text{total})} = (5.3^{+3.6}_{-3.0})\% . \qquad (7)$$

If we take the present[27] upper limit on the X^0 total width: $\Gamma(X^0 \to \text{total}) < 4$ MeV, the corresponding upper limit for the partial width is:

$$\Gamma(X^0 \to 2\gamma) < (220^{+140}_{-120}) \text{ keV} .$$

7. THE INTEREST OF THE X^0 DECAY $\to 2\gamma$

Remember that the partial width of the η into two gammas may be predicted using SU(3) symmetry, knowing the partial width of $\pi^0 \to 2\gamma$, i.e. the π^0 lifetime:

$$\frac{\Gamma(\eta \to \gamma\gamma)}{\Gamma(\pi^0 \to \gamma\gamma)} = \left(\frac{m_\eta}{m_{\pi^0}}\right)^3 \times \frac{1}{3} .$$

The factor of three is because the isovector spin coupling to the electromagnetic field is a factor of three stronger than the isoscalar coupling. Taking the known π^0 lifetime, one calculates an expected $\Gamma(\eta \to \gamma\gamma)$ of about 160 eV. As mentioned above, a very nice experiment by the Pisa-DESY Collaboration[25] using the Primakoff effect, has shown without any question that the value is by no means 160 but is

$$\Gamma(\eta \to \gamma\gamma) = (880 \pm 190) \text{ eV} .$$

Now we know that SU(3) is violated but we have never seen anything like this tremendous violation; so, what happens? Is the η mixed or is it a pure state?

From the Gell-Mann - Okubo mass formula, the $(\eta - X^0)$ mixing is small, about 10° if one uses a quadratic mass formula. Then in order to explain the large value for the width $\Gamma(\eta \to \gamma\gamma)$ and the small $(\eta - X^0)$ mixing, a large width

$\Gamma(X^0 \to \gamma\gamma)$ is predicted. Theoretical predictions are model-dependent and range from 1% to 10% for the branching ratio[28-31].

In spite of the large range of variation, the theoretical predictions have a common interesting feature: the value of BR cannot be very small if the measured value[25] of $\Gamma(\eta \to \gamma\gamma)$ is to be reconciled with SU(3) and with the small $(\eta - X^0)$ mixing. This feature is confirmed by our experimental data.

As is well known[32], a measurement of $\Gamma(X^0 \to \gamma\gamma)$ would provide [when compared with $\Gamma(\eta \to \gamma\gamma)$] an answer to the old problem of the validity of the linear or quadratic mass formula for the mesons. Unfortunately, only an upper limit exists[27] for the absolute width of the X^0, so it is impossible to solve this problem directly from our result (7). In order to attempt to give an answer, it is necessary to use a model. If we compare our result (7) with a current algebra calculation of Baracca and Bramon[30], our data favour the quadratic mass formula with respect to the linear mass formula by a factor of 15 to 1.

O. Goussu, G. Smadja and G. Kayas, Nuovo Cimento 47 A, 383 (1967).

5) O.I. Dahl, L.M. Hardy, R.I. Hess, J. Kirz and D.H. Miller, Phys.Rev. 163, 1377 (1967).

M.A. Abolins, O.I. Dahl, J.S. Danburg, D. Davies, P. Hoch, J. Kird, D.H. Miller and R. Rader, Proc.Int.Conf. on Elementary Particles, Heidelberg (1967), p. 509; and private communication.

G.H. Boyd, A.R. Erwin, W.D. Walker and E. West, Phys.Rev. 166, 1458 (1968).

6) M. Gell-Mann, Phys.Rev. 125, 1067 (1962); see also Cal.Tech. Report, CTSL-20 (1961) (unpublished).

7) Y. Ne'eman, Nuclear Phys. 26, 222 (1961).

8) S. Okubo, Progr.Theor.Phys. (Kyoto) 27, 949 (1962).

R.P. Feynman suggested the use of $(\text{mass})^2$ for bosons.

9) J.J. Sakurai, Phys.Rev.Letters 9, 472 (1962).

10) J.J. Sakurai, Phys.Rev. 132, 434 (1963).

11) S. Okubo, Phys.Rev.Letters 5, 165 (1963).

12) S.L. Glashow, Phys.Rev.Letters 11, 48 (1963).

13) S. Coleman and H.J. Schnitzer, Phys.Rev. 134 B, 863 (1964).

14) N.M. Kroll, T.D. Lee and B. Zumino, Phys.Rev. 157, 1376 (1967).

15) T. Das, V.S. Mathur and S. Okubo, Phys.Rev. Letters 19, 470 (1967).

16) R.J. Oakes and J.J. Sakurai, Phys.Rev.Letters 19, 1266 (1967).

17) S. Weinberg, Phys.Rev.Letters 18, 507 (1967).

18) R. Van Royen and V.F. Weisskopf, Nuovo Cimento 50 A, 617 (1967).

19) D. Bollini, A. Buhler-Broglin, P. Dalpiaz, T. Massam, F. Navach, F.L. Navarria, M.A. Schneegans and A. Zichichi, Nuovo Cimento 56 A, 1173 (1968) and 57 A, 404 (1968).

20) U. Becker, W.K. Bertram, M. Binkley, C.L. Jordan, T.M. Knasel, R. Marshall, D.J. Quinn, M. Rohde, A.J.S. Smith and S.C.C. Ting, Phys.Rev.Letters 21, 1504 (1968).

21) J.E. Augustin et al., Phys.Letters 28 B, 508 (1969); ibid. 28 B, 513 (1969); ibid. 28 B, 517 (1969).

22) A. Baracca, Nuovo Cimento 60 A, 633 (1969).

23) J.B. Bronzan and F.E. Low, Phys.Rev.Letters 12, 522 (1964).

24) D. Bollini, A. Buhler-Broglin, P. Dalpiaz, T. Massam, F. Navach, F.L. Navarria, M.A. Schneegans and A. Zichichi, Nuovo Cimento 58 A, 289 (1968).

25) C. Bemporad, P.L. Braccini, L. Foà, K. Lübelsmeyer and D. Schmitz, Phys.Letters 25 B, 380 (1967).

26) M.A. Abolins, O.I. Dahl, J. Danburg, D. Davies, P. Hoch, J. Kirz, D.H. Miller and R. Rader, Proc.Int.Conf. on Elementary Particles, Heidelberg (1967), p. 509; and private communication.

27) P.M. Dauber, W.E. Slater, L.T. Smith, D.H. Stork and H.K. Ticho, Phys.Rev.Letters 13, 449 (1964).

28) R.H. Dalitz and D.G. Sutherland, Nuovo Cimento 37, 1777 (1965).

29) M. Jacob, CERN Internal Report, TH/846-1967.

30) A. Baracca and A. Bramon, Nuovo Cimento 53 A, 571 (1968.

31) F. Guerra, F. Vanoli, G. De Franceschi and V. Silvestrini, Phys.Rev. 166, 1587 (1968).

32) See, for instance, the review talk of H. Harari at the Symposium on the Present Status of SU(3) for Particle Couplings and Reactions, July 1967, Argonne National Laboratory.